Effect of a uniform magnetic field on corrosion of Ni-Al bronze in 3.5 wt% NaCl

Hedda Nordby Krogstad*[a], Roy Johnsen[a] & Michael Coey[b]

[a]*Department of Mechanical and Industrial Engineering, NTNU*
[b]*School of Physics, Trinity College Dublin*

Keywords: Ni-Al Bronze, magnetic field, 3.5. wt% NaCl

[a] MTP Gloeshaugen, Richard Birkelands vei 2B, 7491 Trondheim, Norway
[b] Trinity College Dublin, College Green, Dublin 2, Ireland

*Corresponding author:
Tlf: 0047 906 05 873
Email: hedda.krogstad@ntnu.no.

ABSTRACT

Following the observation of enhanced corrosion of parts of a seawater-immersed permanent magnet motor made from Ni-Al bronze, a laboratory study of the effect of uniform magnetic field on the corrosion of this alloy in a 3.5 wt% NaCl solution has been carried out. The results have been compared with measurements of enhanced convection with a rotating disc electrode. The largest effect of the magnetic field was an enhancement of the anodic current density of 52 % in a field of 800 mT. This enhancement was equivalent to that due to gentle stirring with the rotating disc electrode with diameter 10 mm at 20 rpm. The increase in corrosion current varied with the magnitude of both the magnetic field and the initial corrosion current, and increased with both. The effect can be explained in terms of the Lorentz force, and modelling was performed to quantify the flow induced in the electrolyte by this force.

INTRODUCTION

Magnetoelectrochemistry is concerned with the effect of a magnetic field on electrochemical systems. The approach within this field has mainly been to investigate the effect of uniform magnetic fields on the limiting current density in mass-transport controlled systems [1–5], or to use activation controlled systems to identify any effect on charge transfer kinetics [6]. Well known electrochemical systems have often been chosen for the experimental work in order to minimize the complexity of the experiments. Examples of such electrochemical systems are pure metals (e.g. Cu or Fe) in acidic solutions [7–10], or inert electrodes in redox solutions [11,12]. This approach has been essential for understanding the fundamental effects of a magnetic field on electrochemical reactions, and has brought valuable information to the field of magnetoelectrolysis. Two early review articles by Fahidy [13] and Tacken & Janssen[14] summarize most of the work done up till 1995.

The motivation behind the work presented in this paper was to investigate whether a magnetic field can accelerate the corrosion of anodically polarized Ni-Al bronze (UNS C95800) in seawater, and if so, to quantify the effect. The work was initiated after incidents where Ni-Al Bronze suffered high-rate corrosion in close proximity to a magnetic field in a permanent magnet motor operating in seawater. It is known that the corroded Ni-Al Bronze was anodically polarized due to galvanic

coupling to stainless steel. This galvanic effect has been extensively studied in previous works by the author [15,16]. Under slowly flowing conditions (< 1 cm/s) the coupled potential stabilized at -50 mV vs. the saturated Ag/AgCl/KCl electrode (referred to as Ag/AgCl from this point), and the galvanic current density ranged from 0.06 – 11 A/m² depending on the area ratio of the galvanic couple. The range of potentials and corresponding current densities in this work are chosen to accommodate the values found in the previous work.

Magnetic forces in electrochemical systems

Although the dawn of magnetoelectrolysis was Faraday's unsuccessful attempt in 1832 to detect a potential difference across the river Thames due to its flow in the Earth's magnetic field [17], most of the results have been generated since the 1970s. Several works emphasize the effect of a magnetic field on mass transport and explain the effect by two different forces: The Lorentz force [11,13,18–25] and the Kelvin (or field gradient) force [12,26–28]. The former is due to the interaction of the magnetic field with the electric currents flowing in the electrolyte, while the latter depends on the magnetic properties of the electrodes and the species dissolved in the electrolyte. A more thorough introduction to each of these forces is given below. A limited number of papers deal with the effect of magnetic fields on charge transfer [6,20]. Several papers conclude that regarding Cu, which is the main constituent of Ni-Al Bronze, a magnetic field has no effect on the charge transfer coefficients [20,29–32].

The Lorentz force: If a charge is moving in a magnetic field, it will experience a force normal to the direction of both its movement and to the direction of the magnetic field. This is called the Lorentz force. For a negative and positive charge moving in opposite directions, the force will be in the same direction. As the paths of the ions are altered and aligned under the influence of the Lorentz force, the movement is transferred to the electrolyte through viscous forces, and convection (flow) is induced [30]. The mathematical description of the Lorentz force is according to Equation (1):

$$F_L = i \times B \qquad (1)$$

Here, F_L is a body force with the unit N/m³, i is the current density in A/m² and B is the magnetic flux density in Tesla, T. The magnitude of the Lorentz force is hence dependent on the strength of the magnetic field, the current density flowing in the system, and the orientation of the field with respect to the current density (which is normal to the electrode surface). A schematic illustration of the Lorentz force is provided in FIGURE 1.
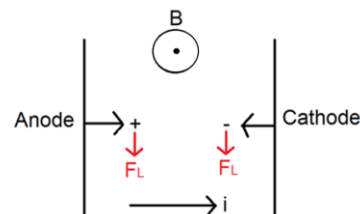

FIGURE 1: *Schematic illustration of the direction of the Lorentz force, F_L, on charges moving outward from the anode and the cathode in an electrolyte where a magnetic field B is applied parallel to the electrode surfaces.*

In electrolytes that are not stirred by other means, the flow induced by the Lorentz force will interfere with the diffusion layer thickness, and the transportation of species to and from the electrode surfaces will be accelerated [13]. If the electrochemical system under study is under mass transport or mixed control, and there are no inhibitors present, the effect of the magnetic field will be higher current densities. Several authors have reported increased limiting current densities under the

influence of magnetic fields [11,13,30]. Aaboubi et al. [19] showed that the limiting current density is proportional to $B^{1/3}c^{4/3}$, where c is the concentration of electroactive species.

The Kelvin Force (field gradient force): Magnetic field gradients exist naturally around every magnet, causing diamagnetic and paramagnetic species to move away from and towards regions of higher magnetic field strength, respectively [33]. Even in a uniform magnetic field, field gradients arise if ferromagnetic electrodes are placed inside the field. The reason is that the permeability of ferromagnetic materials is much higher than that of the surrounding air or electrolyte, and the magnetic flux lines close to the electrode will be diverted into the electrode [27,34]. The expression for the field gradient force F_K (N/m³) on the species in the electrolyte is according to Equation (2):

$$F_K = (1/2\mu_0)\,\chi_m c\nabla B^2 \tag{2}$$

Where χ_m is the molar magnetic susceptibility of the electrolyte (m³/mol), c is the concentration of magnetic species (mol/m³) and μ_0 is the permeability of free space ($4\pi\,10^{-7}$ Am²/T) [35]. This force may interfere with mass transport of reactants and products. However, unless an electrode is designed specifically to create a large field gradient ($\nabla B \gg 1$ T/m), such as ferromagnetic micro-electrodes, this force has limited influence on the overall mass transport [36]. The field gradient force is minimized in this work by performing experiments between the poles of a large electromagnet where the field is highly uniform in the volume occupied by the test cell. The working electrode, however, is made of Ni-Al Bronze, which is weakly ferromagnetic due to the content of Ni and Fe.

Some papers also refer to a paramagnetic force, arising when paramagnetic species accumulate on the surface of an electrode, creating a higher magnetic susceptibility in this region compared to the surrounding bulk [23,37]. However, Coey and Dunne [38] have shown that there is no significant body force associated with ionic concentration gradients for electrochemical systems in a uniform magnetic field. However, the Kelvin force can create local convective flow when there is a magnetic field gradient with a component perpendicular to a concentration gradient that exists, for example, in the diffusion layer [35], as shown in Equation (3):

$$\nabla \times F_K = (1/2\mu_0)\chi_m(\nabla c \times \nabla B^2) \tag{3}$$

Hinds et. al [36] have summarized the forces acting on an electrolyte, see Table 1.

Table 1: Forces acting in an electrolyte after Hinds et al. [36]. Typical values are inserted into the equations, and are listed at the bottom row of the table.

Force	Expression	Typical value [N/m³]
Driving force for diffusion	$RT\nabla c$	10^{10}
Driving force for migration	$zFc_\infty\nabla V$	10^{10}
Driving force for forced convection	$\rho(r\omega)^2/2\delta_0$	10^5
Driving force for natural convection	$\nabla\rho g$	10^3
Viscous drag	$\eta\nabla^2\boldsymbol{u}$	10^2
Kelvin force (field gradient force)	$\chi_m c\nabla B^2/\mu_0$	10^1
Lorentz force	$\boldsymbol{j}\times\boldsymbol{B}$	10^3
(R= 8.31 kg m²/s²Kmol, T=298 K, c = 10^3 mol/m³, z=2, V= 1V, ρ= 10^3 kg/m³, d= 10^{-2} m, ω= 10^2 rad/s, δ_0= 10^{-3} m, $\nabla\rho$= 10^2 kg/m³, η= 10^{-3} Ns/m², u= 10^{-1} m/s, B= 1T, χ_m= 10^{-8} m³/mol, ∇B= 1T/m, j= 10^3 A/m²)		

From Table 1, it can be seen that the driving forces for diffusion and migration are dominant. The Lorentz force in a field of 1 T is comparable in size to the force driving natural convection.

To summarize: when investigating the effect of a magnetic field on a specific electrochemical system, there are some basic characteristics of the system one need to be aware of:

- Magnetic properties of electrodes and ions in the electrolyte: ferro-, dia- or paramagnetic?
- Orientation of the field with respect to the electrode surface: parallel, perpendicular or at an angle?
- Strength and spatial distribution of the magnetic field: how strong and uniform is the field?
- What current densities are flowing in the system?
- Is the electrochemical system under activation, mixed or mass transport controlled regime?

Nickel-Aluminium Bronze

Ni-Al Bronze includes a range of Cu-based alloys containing 9-12 wt% aluminium with additions of up to 6 wt% each of Fe and Ni [39]. In this work the alloy UNS C95800 according to EN[(1)] 1982:2008 with nominal composition Cu-10Al-5Ni-5Fe has been used. Due to the presence of Ni and Fe this alloy is ferromagnetic with a weak room-temperature saturation magnetization M_s = 28 kA/m. For comparison, the M_S of metallic Fe and Ni are 1 745 and 521 kA/m, respectively [40]. The alloy has a complex microstructure, with intermetallic particles named κ_I- κ_{IV} distributed unevenly in a Cu-rich matrix. The intermetallic particles differ in shape, composition and size, and most of the Fe is found in spherical, discontinuous particles with a size ranging from < 2 μm (κ_{IV}), to 50 μm (κ_I) [41]. Most of the Ni is found in narrow (5-10 μm), continuous lamellas (κ_{III}) [42]. Due to a significant difference in the nobility of the phases in Ni-Al Bronze, the alloy is susceptible to selective corrosion [16,39]. Upon immersion in fresh, natural seawater the Cu rich matrix adjacent to the lamellar k_{III} is known to be preferentially attacked through oxidation of Cu by Cl⁻ to form predominantly $CuCl_2^-$ [42–45]. The corrosion behavior of Ni-Al Bronze is therefor similar to that of unalloyed Cu under these conditions [43,46,47]. The anodic dissolution of Cu follows a tafel-like behavior in the lower range of anodic overpotentials, where mixed charge transfer and mass transport kinetics are assumed [47]. Under stagnant conditions, $CuCl_2^-$ accumulates in the electrolyte adjacent to the electrode surface, decreasing the dissolution rate as the equilibrium between Cu, Cl⁻ and $CuCl_2^-$ is altered. If flow is induced in the electrolyte, $CuCl_2^-$ is removed faster from the electrode surface as the diffusion layer thickness decreases, allowing the continued dissolution of Cu to remain high [48,49]. If the saturation limit of $CuCl_2^-$ is reached in the electrolyte adjacent to the sample surface, a film of solid CuCl precipitates [48,50,51]. The CuCl film provides some protection against dissolution, and causes a deviation in the tafel-like behavior of the anodic polarization curve of Cu (and Ni-Al Bronze) in chloride containing

---

(1) EN: European Standard EN 1982:2008, Cu Alloys – ingots and castings

electrolytes upon precipitation (observed as a decrease in current density) [47]. During short-time exposure, the behavior of Ni-Al bronze in seawater and 3.5 wt% NaCl is assumed to be comparable. Schüssler et. al[52] reported the main difference between the behavior of Ni-Al bronze in 3.5 wt% NaCl and synthetic seawater (ssw) was an initially higher corrosion current in 3.5 wt% NaCl compared to ssw. Additionally, the buffer capacity of seawater and 3.5. wt% NaCl differ significantly, which plays a role in formation and composition of a mature oxide film during longer exposure times of Ni-Al bronze [52]. Long-time exposure is however out of the scope of the work presented here.

Experimental Procedure

The main goal of this work was to investigate whether or not a uniform magnetic field can accelerate the corrosion rate of anodically polarized Ni-Al Bronze. Knowing that a magnetic field can induce flow in a stagnant electrolyte when current is flowing, knowledge about the effect of flow on anodically polarized Ni-Al Bronze was necessary to establish. This knowledge was provided by performing tests with a rotating disk electrode (RDE) in absence of any applied magnetic field. The effect of a magnetic field on anodically polarized Ni-Al Bronze was investigated by performing electrochemical tests between the poles of a large electromagnet in a glass cell under stagnant conditions. All experiments were performed on freshly prepared samples, i.e. polished samples exposed for a maximum of 30 minutes to the electrolyte before the electrochemical test was initiated. The tests were performed at room temperature (22 ± 2^0C). The Ni-Al Bronze used in all tests was taken from one of the corroded permanent magnet motors, and the composition is given in Table 2.

Table 2: Composition of the Ni-Al Bronze (UNS C95800) used in the experimental work.

Element	Cu	Al	Ni	Fe	Mg	Mn
wt%	80,5	9,4	5,0	4,3	< 0,01	0,7
Element	Cr	Si	Zn	Sn	Pb	Mn
wt%	< 0,005	0,015	0,03	0,01	< 0,01	0,7

Three techniques were applied to investigate the effect of rotation rate (in the RDE test set-up), and uniform magnetic field (in the electromagnet test set-up), on the corrosion behavior of Ni-Al Bronze: i) anodic polarization curves, ii) potensiostatic polarization to fixed anodic potentials and iii) cyclic voltammetry. Details about each test in the RDE and electromagnet test set-ups are provided below, and summarized in Table 3.

Tests conducted with a rotating disk electrode: The test sample, a solid rod 50 mm long and 10 mm in diameter was produced in Ni-Al Bronze. The outer diameter rod surface was roughened with 240 grit SiC paper and painted with a two-component epoxy paint (Jotamastic 87[(2)]). One end of the rod was threaded to fit into the rotating instrument, while the other end was polished with 600 grit SiC paper. The RDE test sample, i.e. the working electrode (WE), was mounted vertically on the rotating instrument (Pine[(3)] Research Rotator). The RDE was exposed to an electrolyte made from distilled water with 3.5 wt% NaCl (pH 6.6) in a 1L glass container. A platinum counter electrode and a salt bridge connecting a saturated Ag/AgCl/KCl reference electrode completed the RDE test-set-up.

Anodic polarization curves (i) were recorded at 0, 50 and 800 revolutions per minute (rpm) with a scan rate of 10 mV/min. The sample was left 10 min at open circuit potential (OCP) with the respective rotation rate before the curves were recorded from OCP to OCP+300 mV.

Five anodic potentials were chosen for the *potensiostatic polarization tests* (ii): -180, -155, -130, -50 and -25 $mV_{Ag/AgCl}$ (OCP was in the range of -210$\pm$5 $mV_{Ag/AgCl}$). During the test, the sample was kept at one of the chosen anodic potentials during the full test period (1 h) and the anodic current was measured. The sample was left 10 minutes to stabilize a base current density, i_b, at zero rpm, before increasing the rotation rate stepwise every second minute. The rotation rates applied were 50, 100, 200, 400, 600, 800 rpm. Two repeats were conducted for each experiment. A similar approach was applied to examine the effect of rotation rate on OCP (one sample/no repeat). To examine the effect of lower rpm on the anodic current density, one sample anodically polarized to -50 $mV_{Ag/AgCl}$ was subject to rotation rates in the range 0-50 rpm, stepping up the rate by 10 rpm every second minute (one sample/no repeat).

For the *cyclic voltammetry (iii)*, the sample was subject to cyclic polarization from -700 $mV_{Ag/AgCl}$ to + 300 $mV_{Ag/AgCl}$ and back to -700 $mV_{Ag/AgCl}$ at a scan rate of 50 mV/s. A total amount of 25 cycles were run, and during the first 5 cycles the RDE was not rotating (0 rpm). After 5 cycles, the rotation rate was increased to: 10, 20, 30, 40, 50, 100, 200, 400, 800 and 1,600 rpm sequentially. At each rotation rate, two voltammetry cycles were recorded.

Test conducted between the poles of the electromagnet: Samples of Ni-Al Bronze with 28 mm diameter and 4 mm thickness were used. The samples were sandblasted and painted (Jotamastic 87) on all sides, before polishing one of the flat surfaces with 600 grit SiC paper. For electrical connection and mounting purposes, a stainless steel wire 50 mm long, and 1.6 mm in diameter was inserted radially into a drilled hole and fixed to the sample. The stainless steel wire was then covered with heat-shrinkable polymer tubing and silicon in the joints to prevent the wire from being in contact with the electrolyte. A platinum sheet with dimensions 10x15x0.25mm was used as a counter electrode (CE). The CE was fixed to a stainless steel wire in a similar manner as the Ni-Al Bronze working electrode, but instead of inserting the wire into the CE, the CE was inserted into a small cut across the diameter of the wire. The stainless steel wire was covered with heat-shrinkable polymer tubing and silicon in the joints to prevent the wire from being in contact with the electrolyte. Fixing the WE and CE to stiff wires made it easier to mount the electrode in the test-cell. The test-cell used for the experiments was custom made in glass to fit in the 40 mm gap between the poles of the electromagnet. The glass cell had a cylindrical shape, with a diameter of 100 mm and 35 mm width. The glass cell held 0.2 l of electrolyte made from deionized water with 3.5 wt% NaCl (pH 6.3). After mounting the electrodes into the glass cell by inserting the stainless steel wires through a tight hole in rubber caps, the polished surface of the sample was facing the CE and oriented perpendicular to the surface of the magnetic poles in the electromagnet. In this configuration the Lorentz force will be at a maximum as the magnetic field lines are perpendicular to the vector of current density, ref. Equation (1). The poles of the electromagnet were 200 mm in diameter, giving a highly uniform magnetic field inside the test-cell. During the tests the field was continuously measured by a Gaussmeter (Transverse probe, Hirst[(4)]

Magnetic Instruments). A minimum of two repeats were conducted for each electrochemical test, unless stated otherwise.

The *anodic polarization curves* (i) were recorded from OCP to OCP+500 mV with a scan rate of 20 mV/min. Slower scan rates were not possible because of excessive heating of the electromagnet when applying the highest magnetic field. Curves were recorded under three different conditions: i) 0 mT, ii) 300 mT and iii) 1,000 mT. The sample was left 10 min at OCP prior to recording the curves, with no magnetic field applied. All curves were recorded with the sample placed in the glass cell between the poles of the electromagnet, with the sample surface perpendicular to the surface of the poles of the electromagnet.

For the *potensiostatic polarization* (ii), six anodic potentials were chosen: -180, -155, -130, -90, -50 and -25 mV$_{Ag/AgCl}$ (the OCP was in the range of -210±7 mV$_{Ag/AgCl}$). The sample was polarized to one of the six potentials and for the first 30 minutes, no magnetic field was applied and the current density stabilized. After 30 min, the magnetic field was set to 25 mT and then increased every 4 minutes to the following values: 50, 100, 200, 400, 600 and 800 mT, before the magnetic field was turned off.

For the *cyclic voltammetry* (iii), the sample was subject to cyclic polarization from -700 mV$_{Ag/AgCl}$ to + 300 mV$_{Ag/AgCl}$ and back to -700 mV$_{Ag/AgCl}$ at a scan rate of 50 mV/s. A total amount of 15 cycles was run, and during the first 5 cycles, no magnetic field was applied. After 5 cycles, magnetic field intensities of 100, 200, 400, 600 and 800 mT were applied sequentially. At each field intensity, two voltammetry cycles were recorded.

To examine the influence of a magnetic field on the OCP, the magnetic field was in several test increased while measuring OCP. No effect could be detected in the range of magnetic fields applied in this work. One test where the field was increased up to 1,500 mT for a short period of 2 minutes was therefore performed. Table 3 gives a summary of the experimental details for test i), ii) and iii) in the RDE set-up and for the electromagnet set-up

Table 3: Experimental details.

	RDE set-up	Electromagnet set-up
i) Anodic polarization curves	**Scan rate:** 10 mV/min **Scan limits:** OCP+300 mV **Rotation rates:** 0, 50 and 300 rpm **Repeats:** 2	**Scan rate:** 20 mV/min **Scan limits:** OCP+500 mV **Magnetic fields:** 0, 300 and 1000 mT **Repeats:** 2 or more
ii) Potensiostatic polarization	**Potentials:** -180, -155, -130, -50, -25 mV$_{Ag/AgCl}$ **Rotation rates:** 0, 50, 100, 200, 400, 600, 800 rpm **Hold time at 0 rpm (to stabilize i$_b$):** 10 min **Time between increase in rpm**: 2 min **Repeats:** 2	**Potentials:** -180, -155, -130, -90, -50, -25 mV$_{Ag/AgCl}$ **Magnetic fields:** 0, 25, 50, 100, 200, 400, 600, 800 mT **Hold time at 0 field (to stabilize i$_b$):** 30 min **Time between increase in B:** 4min **Repeats:** 2
iii) Cyclic voltammetry	**Scan rate:** 50 mV/s **Scan limits:** OCP(start), +300mV$_{Ag/AgCl}$ (max) and -700 mV$_{Ag/AgCl}$(minimum)	**Scan rate:** 50 mV/s **Scan limits:** OCP(start), +300 mV$_{Ag/AgCl}$ (max) and -700 mV$_{Ag/AgCl}$(minimum)

|	Rotation rates: 0, 10, 20, 30, 40, 50, 100, 200, 400, 800 and 1,600 rpm	Magnetic fields: 0, 100, 200, 400, 600 and 800 mT
	Total number of cycles: 25	**Total number of cycles:** 15
	Cycles at rotation rate = 0 rpm: 5	**Cycles at B = 0 mT:** 5
	Cycles at rotation rate > 0 rpm: 2	**Cycles at B > 0:** 2

Modelling induced flow due to the Lorentz force. It was problematic to measure induced flow in the electrolyte when the glass cell was placed between the poles of the electromagnet due to several reasons: non-uniform flowrate in the glass cell, lack of line-of-sight, and a strong stray magnetic field putting cameras in danger of demagnetization. Therefore, modelling in 3D with appropriate software was performed, in an attempt to quantify the flow induced by the Lorentz force. Comsol Multiphysics[5] was chosen for this purpose. Representative images of the test set-up as described in the software are presented in FIGURE 2. The anodic current density of Ni-Al Bronze was set to the values recorded at each anodic potential in test ii) in the electromagnet tests described above. The flow induced by applying a magnetic field parallel to the exposed surface was simulated for field intensities of 25, 50, 100, 200, 400, 600 and 800 mT. The dynamic viscosity of the electrolyte was set to 0.001 Pa/s, the density 1,000 kg/m^3 and the conductivity 3 S/m. Temperature was not included as a variable, and kept constant at 22°C. The Lorentz force is calculated as the cross product between the vectors of current density and magnetic flux according to Equation (1). If the magnetic field is applied only in the z direction (see FIGURE 2), the volume force **F** on the charge carriers in the electrolyte is according to Equation (3):

$$\boldsymbol{F} = \boldsymbol{i} \times \boldsymbol{B} \rightarrow \begin{vmatrix} \boldsymbol{x} & \boldsymbol{y} & \boldsymbol{z} \\ i_x & i_y & i_z \\ 0 & 0 & B_z \end{vmatrix} = \boldsymbol{x} \left| i_y B_z \right| - \boldsymbol{y} \left| i_y B_z \right| \quad (3)$$

Here, **x**, **y** and **z** are unit vectors. Once the force is calculated, the induced flow is calculated by the software through the Navier Stokes equation, Equation (4):

$$\rho \left(\frac{\partial \boldsymbol{u}}{\partial t} + \boldsymbol{u} \cdot \nabla \boldsymbol{u} \right) = -\nabla p + \nabla \cdot (\mu (\nabla \boldsymbol{u} + (\nabla \boldsymbol{u})^T) - \frac{2}{3} \mu (\nabla \cdot \boldsymbol{u}) I + \boldsymbol{F} \quad (4)$$

Where $\boldsymbol{u}$ is the fluid flow velocity in m^2/s, ρ is the fluid density in kg/m^3, μ is the fluid dynamic viscosity in Pa s, p is the fluid pressure in Pa and $\boldsymbol{F}$ is the external forces in N/m^3 applied to the fluid (Lorentz force in this case).
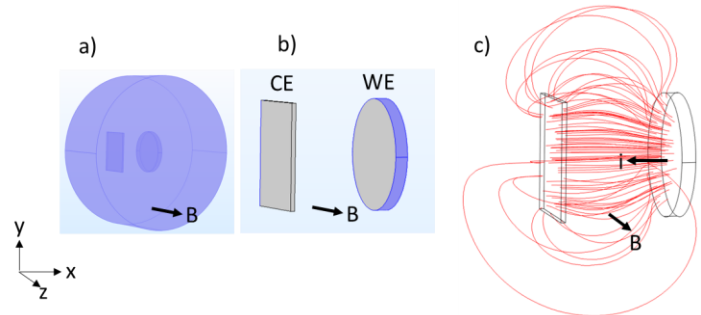
FIGURE 2: *The test-cell with working (WE) and counter (CE) electrodes. a) the cell filled with electrolyte, b) a detailed view of the electrodes,*

*and c) the current flowing in the electrolyte during anodic polarization with the direction of **i** and **B** indicated.*

Results and discussion
Results from the rotating disk electrode tests.
FIGURE 3 shows the anodic polarization curves (i) recorded at 0, 50 and 800 rpm. The anodic curve shifts to the right, i.e. towards higher current densities, with increasing rotation rate. The relative increase in anodic current density is higher closer to OCP than with increasing anodic overpotentials. This is seen as a larger separation between the curves at the lower overpotentials (from slightly above OCP to approximately -100 mV$_{Ag/AgCl}$). The result clearly shows that freshly exposed Ni-Al Bronze suffers a significant increase in dissolution rate when convection is introduced to the system. This effect is explained in terms of the increased mass transport of CuCl$_2^-$ away from the surface of the working electrode [48,49], as the diffusion layer thickness is inversely proportional to the square root of the rotation rate [53]. Faster removal of CuCl$_2^-$ away from the electrode surface helps maintain the driving force for the anodic reaction high, as the potential for the reaction varies according to the Nernst equation, Equation (5):

$$E_{reaction} = E^0_{reaction} - (RT/F)*ln([CuCl_2^-]/[Cl^-]^2) \qquad (5)$$

Where R is the gas constant, F is Faradays constant, T is the temperature in Kelvin, [CuCl$_2^-$] and [Cl$^-$] represent the concentration of these species. The polarization curve recorded at 0 rpm has a maximum current density of approximately 100 A/m^2, from which point the current density is decreasing with higher potentials. This decrease in current density is attributed to the precipitation a CuCl film at the most active anodic sites [16,47]. For the curves recorded at 50 rpm and 800 rpm no decrease in current density is observed within the scan limits in this work, and this is explained by the increased transportation rate of CuCl$_2^-$, delaying the precipitation of CuCl.
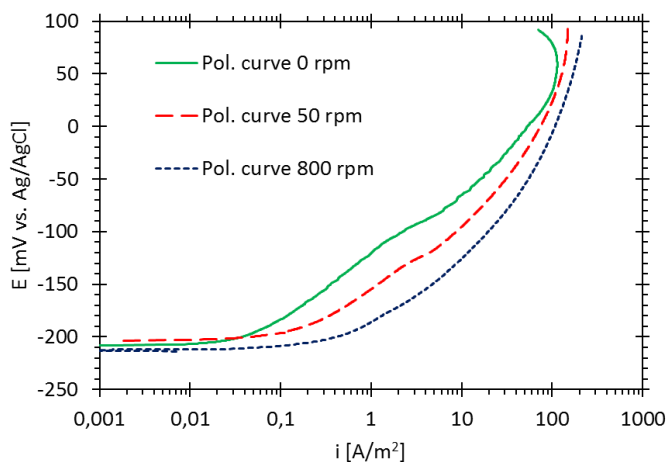

FIGURE 3: *Anodic polarization curves (pol. curve) recorded on Ni-Al Bronze rotating disk electrode at 0, 50 and 800 revolutions per minute (rpm) in a 3.5 wt% NaCl solution.*

The results from the potensiostatic measurements (ii) were plotted as anodic current density versus time, as seen in FIGURE 4 for a sample polarized to -50 mV$_{Ag/AgCl}$ (OCP was -210±7 mV$_{Ag/AgCl}$). A base current density, i$_b$, was calculated for each potential by extrapolating the value of stabilized current density before and after the different rotation rates were applied, see the stippled line in FIGURE 4. The relative increase in current density with rpm was calculated using the average current density at a given rpm and comparing it to the average value of i$_b$ in the same time-period.
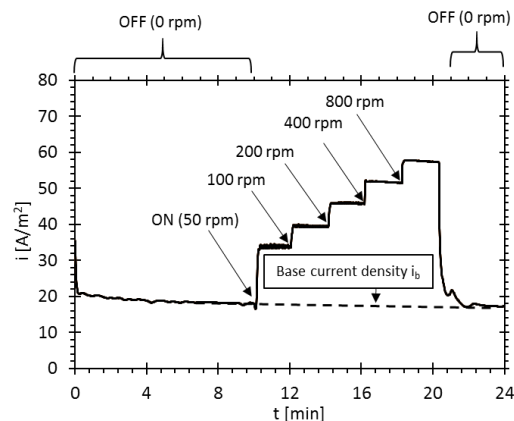

FIGURE 4: *Anodic current density versus time for one of the repeats for Ni-Al Bronze polarized to -50 mV$_{Ag/AgCl}$. Arrows indicate the onset of the specified rotation rate in revolutions per minute (rpm).*

In FIGURE 5, the average percentage increase in current density as a function of i$_b$ is shown for the five potentials and five rotation rates investigated in this work. The results were highly reproducible and standard deviation was at maximum 18.4 %. The current density increases with rotation rate of the disk electrode at all anodic potentials. The relative increase in current density is higher at the lower anodic overpotentials, in accordance with the polarization curves in FIGURE 3. At -180 mV$_{Ag/AgCl}$, the relative increase in current density is 1,865 %, increasing from 0.103 A/m^2 to 2.023 A/m^2 when going from stagnant conditions (0 rpm) to 800 rpm respectively. At -25 mV$_{Ag/AgCl}$, the relative increase in current density was 151 %, increasing from 28.5 A/m^2 to 71.3 A/m^2 when going from 0 to 800 rpm. Hence, the absolute increase in current density increases, while the relative increase is decreasing, with higher polarization potentials.
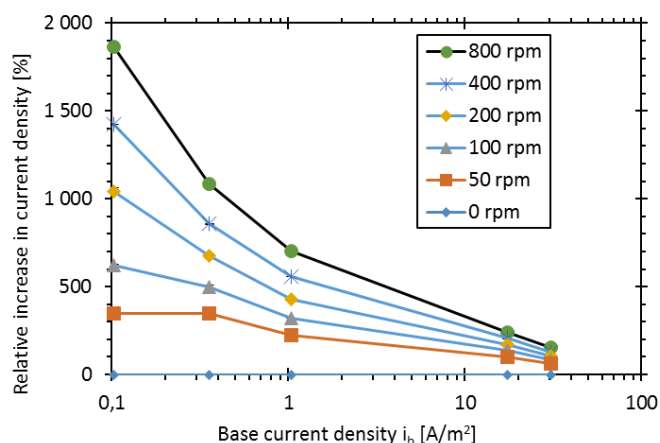

FIGURE 5: *Average relative increase in current density as a function of the base current density i$_b$ at different rotation rates for a Ni-Al Bronze RDE. The anodic potentials are indicated, and are with respect to Ag/AgCl.*

FIGURE 6 a) shows results from the additional test conducted for one sample polarized to -50 mV$_{Ag/AgCl}$ with rotation rates from 0-50 rpm. Close to a 100 % increase in current density is achieved by rotating the electrode at 50 rpm, while a 50 % increase is obtained at roughly 20 rpm, as compared to 0 rpm. In FIGURE 6 b) the measured OCP as a function of rpm is presented. There is a clear trend of a decrease in OCP with

increasing rpm. Wharton and Stokes [42] also reported decreasing OCP with increasing rpm for Ni-Al Bronze in artificial seawater. They attributed this to the mass transport controlled anodic reaction at OCP, while the cathodic reaction is under charge transfer control. This is also supported by Barker et al. [54,55].
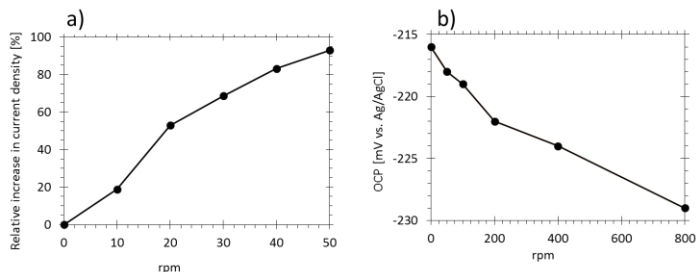

FIGURE 6: *a) Relative increase in current density of Ni-Al Bronze polarized to -50 mVAg/AgCl as a function of rpm. b) OCP of Ni-Al Bronze as a function of rpm.*

In FIGURE 7 the cyclic voltammograms (iii) recorded at various rotation rates are presented. There is no significant effect of the rotation rate on the anodic part of the plot, while there is a significant reduction in the peak cathodic current density on the backscan. This peak is related to the reduction of $CuCl_2^-$ back to Cu and $2Cl^-$ [48] and decreases as the transportation rate of these species away from the surface increases. At 1,600 rpm, the cathodic peak is reduced to a minimum, and the cathodic current on the backward scan is approaching the value representing the oxygen reduction reaction. The lack of any significant effect of rotation rate on the anodic part of the voltammogram is attributed the timescale of the experiment: the scan is too fast for any induced flow to influence the dissolution rate. The curve crosses the y-axis at different potentials on the forward- and backscan: at approximately -210 mV$_{Ag/AgCl}$ on the forward scan, and approximately – 50 mV$_{Ag/AgCl}$ on the backscan. This is attributed to the change in the equilibrium potential as the concentration of $CuCl_2^-$ increases in the electrolyte adjacent to the electrode surface, according to Equation (5). As the rotation rate increases, the equilibrium potential on the backscan is decreasing towards the original OCP, as seen in the insert in FIGURE 7.
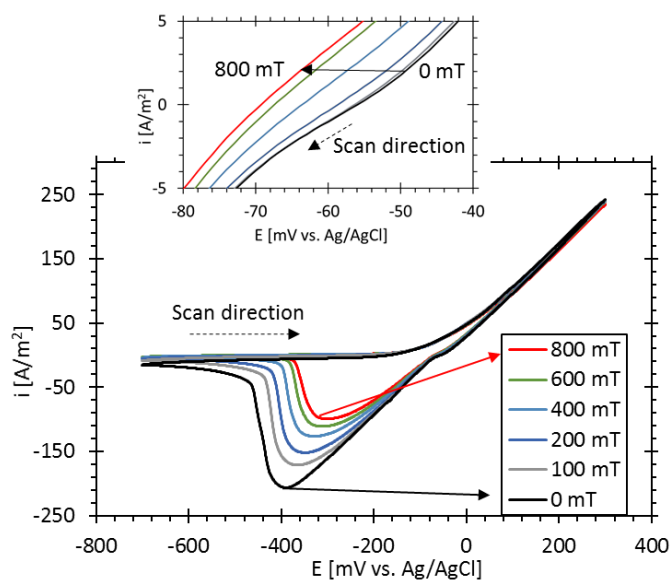

FIGURE 7: *Cyclic voltammogram recorded on Ni-Al Bronze rotating disk electrode rotating at various rotation rates in 3.5 wt% NaCl at a scan rate of 50 mV/s. Insert is a zoom of the potential region where the curve crosses the y-axis on the backscan.*

The results from the RDE experiments emphasize that flow can significantly enhance the dissolution rate of anodically polarized, freshly exposed Ni-Al Bronze.

Results from tests conducted between the poles of an electromagnet
The anodic polarization curves recorded at 0 mT, 300 mT and 1,000 mT are presented in FIGURE 8. The curves overlap from OCP (-210±7 mV$_{Ag/AgCl}$) to approximately -100 mV$_{Ag/AgCl}$, corresponding to current densities of 0.050 - 3 A/m². Above this potential, the curves no longer overlap, and the current density at a given potential increases with increasing magnetic field. This suggests that there is no effect of the magnetic field before the anodic current density exceeds 3 A/m², from which point the there is a gradually increasing effect as the potential is further increased in the anodic direction. The curve recorded in zero field has a current density maximum at approximately 100 A/m², followed by a significant decrease in current density, attributed to the formation of a protective CuCl layer. This is similar to what was observed for the polarization curve recorded at 0 rpm in the RDE experiments (FIGURE 3). The same trend of current density maximum is observed for the curve recorded at 300 mT and 1,000 mT, but at higher potentials, and the following decrease in current density becomes less significant with increasing magnetic field. Both effects of the magnetic field on the polarization curve of Ni-Al bronze; 1) higher dissolution rate once the anodic current density exceeds 3 A/m², and 2) the delayed formation of a protective CuCl film), are explained in terms of increased mass transport as a result of the Lorentz force acting on the moving charges in the electrolyte as described in Equation (1). The induced flow reduces the diffusion layer thickness compared to stagnant conditions, which transports $CuCl_2^-$ faster away from the electrode surface. This will maintain a high driving force for continued dissolution, and delay the saturation limit of the electrolyte to be reached.
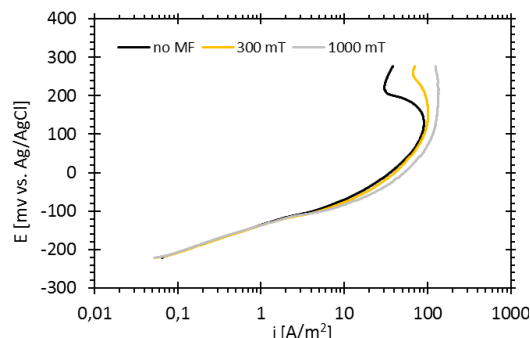

FIGURE 8: *Anodic polarization curves recorded on Ni-Al Bronze in a solution of 3.5. wt% NaCl with a scan rate of 20 mV/min. Curves recorded with a magnetic field of 0, 300 and 1,000 mT oriented parallel to the sample surface.*

The anodic current density of polarized Ni-Al Bronze under influence of a uniform magnetic field of different strengths (ii), is presented in FIGURE 9. The effect of increasing the magnetic field from 0 to 800 mT is an increase in current density readily observed at all potentials. The effect becomes less obvious with the lower current densities (potentials of -155 and -180 mV$_{Ag/AgCl}$) and lower range of magnetic fields (25-200 mT). The only effect observed at these lower current densities and fields strengths is an irregular spike/drop in recorded current density each time the field is changed, indicated with arrows in FIGURE 9. These spikes/drops are attributed to noise due to induction when the magnetic field is increased/decreased.
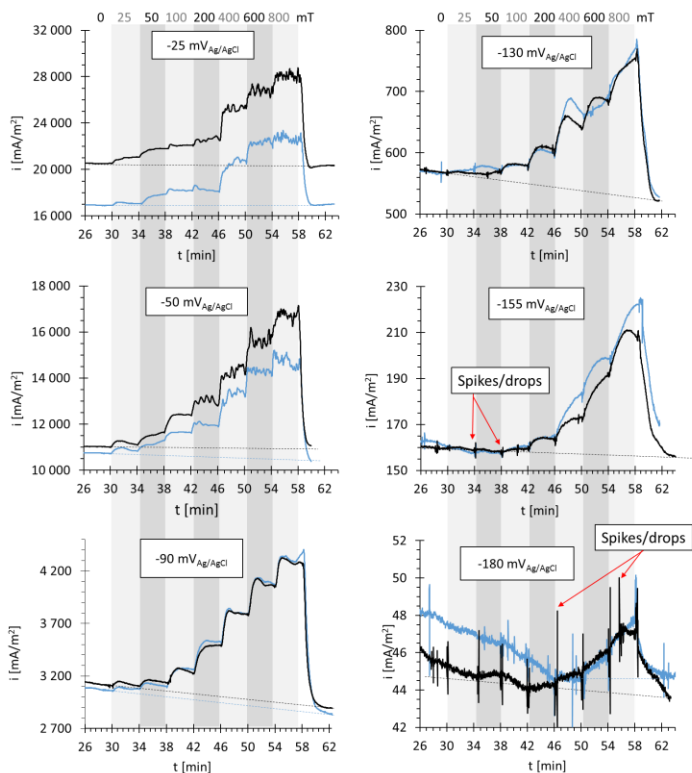
FIGURE 9: *Effect of a uniform magnetic field of 25, 50, 100, 200, 400, 600 and 800 mT (field strength indicated on the top) on the anodic current density of Ni-Al Bronze polarized to -25, -50, -90, -130, -155 and -180 mVAg/AgCl. Stippled lines are estimated base current densities, ib, in zero magnetic field. Arrows indicate examples of sharp spikes/drops in recorded current density at the time when the magnetic field was increased/decreased at the lower anodic potentials.*

Plotting the relative increase in current density as a function of i_b, gives the graph presented in FIGURE 10. This is the same type of plot as presented for in FIGURE 5 for the RDE experiments. The effect of the magnetic field, presented as the relative increase in current density, increases with both increasing magnetic field *and* i_b. Assuming that the relative increase in current density is only related to the flow induced due to interaction between the faradic current flowing in the electrolyte and the magnetic field (The Lorentz force), such a dependency is reasonable, ref. Equation (1). However, a maximum in the relative effect appears to exist at a base current density of 11 A/m² (anodic potential of -50 mV$_{Ag/AgCl}$), as the relative increase in current density at -25 mV$_{Ag/AgCl}$ is less in all fields. Comparing FIGURE 5 and FIGURE 10, the dependency of the relative increase in current density on the rotation rate (in absence of a magnetic field) and magnetic field strength (under stagnant conditions) are the opposite: decreasing with increasing rotation rate, and increasing with increasing magnetic field strength. Only at -25 mV$_{Ag/AgCl}$ the trend with increasing magnetic field follows the trend with increasing rotation rate in FIGURE 5. This will be further discussed in the section where the results from modelling of the flow induced by the Lorentz force is presented.
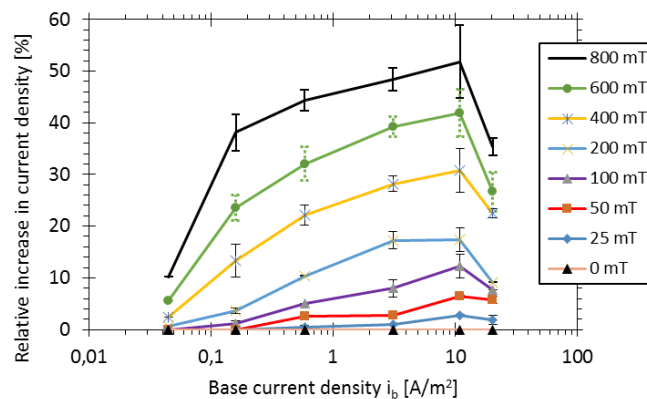

FIGURE 10: *Average relative increase in current density of anodically polarized Ni-Al Bronze in the presence of a magnetic field as a function of the base current density at the respective potentials (vs. Ag/AgCl). The error bars indicate the standard deviation.*

FIGURE 11 shows the development of OCP with and without a magnetic field. As can be seen from the figure only minor fluctuations in OCP are observed during "ramp up" and "ramp down" of the magnetic field. In the time-span where the magnetic field was maintained constant at 1,500 mT, the OCP was unaffected. From this it is concluded that a uniform, static magnetic field up to 1,500 mT has no effect on the OCP of Ni-Al bronze in 3.5 wt% NaCl with the test set-up applied in this work.
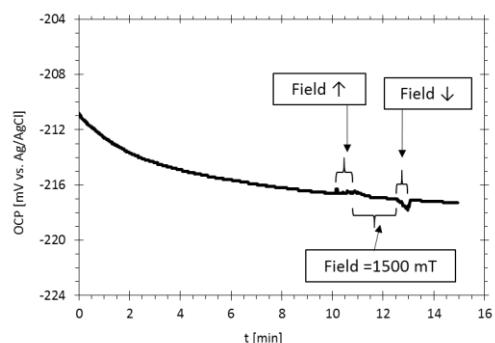

FIGURE 11: *OCP of Ni-Al Bronze in a 3.5 wt% NaCl solution. A magnetic field of 1,500 mT was applied gradually after the 10th minute (Field↑), while the field was decreased back to 0 mT two minutes later (Field ↓).*

The results from the cyclic voltammetry (iii) are presented in FIGURE 12. The anodic curve on the back-scan retraces the anodic curve from the forward scan, indicating that there is no formation of a CuCl film on the sample surface [48]. It does also indicate that there is no effect of the magnetic field on the anodic branch of the voltammogram, similar to the observation made from the cyclic voltammetry performed with the RDE. Youn et al. [49] reported the same (no effect) with a magnetic field of 450 mT on the initial part (i.e. before film-formation by CuCl precipitation) of the anodic branch of their voltammogram of Cu in chloride containing electrolytes. The effect of increasing the magnetic field has the same effect on the cathodic peak current density as increasing the rotation rate in the equivalent RDE experiment (FIGURE 7). The effect is explained in terms of CuCl$_2^-$ being transported away from the electrode surface at a higher rate as the flow induced by the Lorentz force increases with higher magnetic fields strengths. The potential where the curve crosses the y-axis on the backscan (see insert in FIGURE 12) decreases with increasing magnetic field strength (i.e. increasing flow), in accordance with the observations made in FIGURE 7.
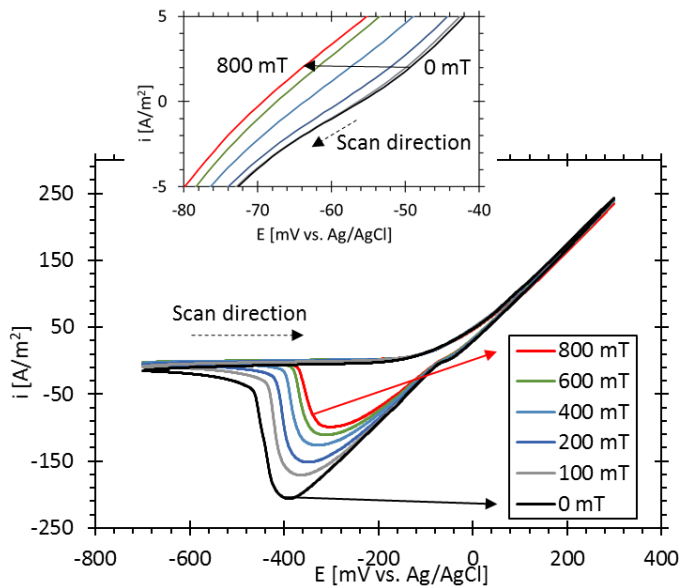
FIGURE 12: *Cyclic voltammogram of Ni Al Bronze recorded at 50 mV/s between -700 and +300mVAg/AgCl in a 3.5 wt% NaCl solution under the influence of different magnetic fields. The insert is a detail of the potential range where the curve crosses the y-axis on the backscan.*

Flow induced by the Lorentz force – results from modelling
FIGURE 13 presents the results from modelling induced flow in the electrolyte for different current densities on an electrode surface oriented parallel to a magnetic field. According to the results, increasing the magnetic field strength at a fixed anodic potential, and increasing the anodic potential at a fixed magnetic field, have a similar effect on how much flow is induced in the electrolyte. This is seen by observing the similar velocity development (indicated by colors) in FIGURE 13 for these two cases.
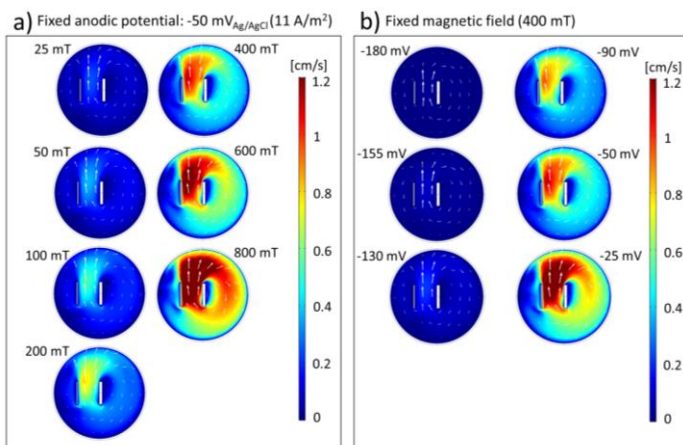

FIGURE 13: *Induced flow (cm/s) in the electrolyte by the Lorentz force when Ni-Al Bronze is anodically polarized while exposed to a uniform magnetic field parallel to its surface. In a): Ni-Al Bronze polarized to -50 mVAg/AgCl (current density 11 A/m2) under the influence of magnetic fields from 25 mT to 800 mT. In b): Ni-Al Bronze polarized to different potentials, under the influence of a fixed magnetic field of 400 mT. See FIGURE 14 for the maximum values of flow.*

The maximum velocity in the electrolyte for each combination of current density (0.045 – 20 A/m²) and magnetic field (25-800 mT) is presented in FIGURE 14, and increases exponentially with the logarithmic scale of

current density. At 800 mT, the highest induced flow is 2.38 cm/s, occurring at the highest base current density in this work (20.5 A/m²).
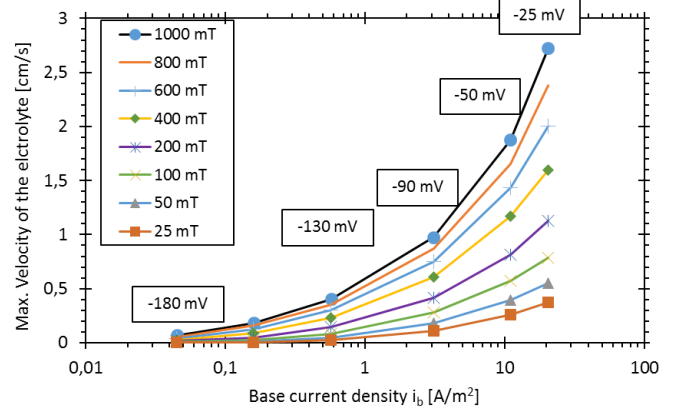

FIGURE 14: *Maximum modelled electrolyte flow velocity from a magnetic field as a function of base current density. The anodic potentials are indicated and are values with respect to Ag/AgCl.*

Because very little flow is induced in the electrolyte by the Lorentz force at low i_b, only a small enhancement of current is obtained. As i_b increases, the induced flow also increases for a given magnetic field, resulting in a larger enhancement of the current density. Plotting the relative increase in current density from FIGURE 10 as a function of the maximum flow induced at each i_b yields the plot presented in FIGURE 15. It is clear from the steep slope for the lowest values of i_b (0.045-0.575 A/m²) that the same sensitivity towards increased flow at the lowest overpotentials reported from the RDE experiments (FIGURE 5) is also valid for the experiments performed in a uniform magnetic field. The decreasing slope of the curves in FIGURE 15 with more positive anodic potential also highlights why the maximum relative effect of the magnetic field was found to be at a potential of -50 mVAg/AgCl in FIGURE 10, despite the fact that maximum induced flow was found at a potential of -25 mVAg/AgCl in FIGURE 14: The increase in induced flow when increasing the polarization potential from -50 to -25 mVAg/AgCl does not compensate for the decrease in sensitivity towards increased flow with increasing potential found in the RDE-results (FIGURE 5), in terms of the relative increase in current density.
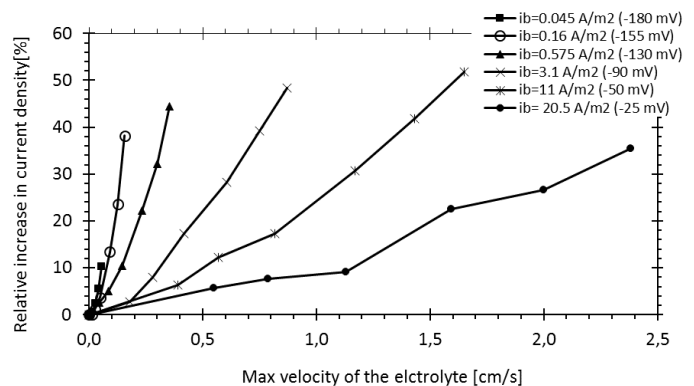

FIGURE 15: *The relative increase in current density for each i_b from FIGURE 10 plotted as a function of maximum induced flow in each magnetic field presented in FIGURE 14.*

The results presented in this work show that freshly exposed Ni-Al bronze will be significantly influenced by convection when anodically polarized in chloride containing media. The convection induced by the

Lorentz force in a uniform magnetic field up to 800 mT will only have an impact on the corrosion of Ni-Al bronze in engineering application involving stagnant or slowly flowing seawater (< 2.5 cm/s). For the permanent magnet motor were Ni-Al bronze suffered high-rate corrosion in close proximity to a magnetic field, this implies that any enhanced corrosion due to the magnetic field must have occurred during periods of stand-still in quiet waters. During periods of operation of the motor, or during stand-still in rough waters, the flow of seawater surrounding the Ni-Al bronze is expected to exceed 2.5 cm/s, and the effect of the Lorentz force will be negligible.

Conclusions

- A uniform magnetic field applied parallel to the corroding surface of freshly exposed anodically polarized Ni-Al Bronze in unstirred solution of 3.5 wt% NaCl will increase the anodic current density.
- The increase in anodic current density is due to induced flow in the electrolyte by the Lorentz force, responsible for increasing mass transport across the diffusion layer.
- The maximum effect of the magnetic field, measured in relative increase in current density was in the order of 50 %. This was comparable to rotating a Ni-Al Bronze disk electrode with diameter 10 mm at 20 rpm.
- The flow induced in the electrolyte was modelled, and a maximum electrolyte velocity of 2.34 cm/s was found for the highest magnetic field (800 mT) and highest polarization potential (-25 mV$_{Ag/AgCl}$) investigated in this work.
- A uniform magnetic field up to 1,500 mT applied perpendicular to Ni-Al Bronze had no effect on the OCP in 3.5 wt% NaCl.

References

1. Chopart, J.-P., Aaboubi, O., Merienne, E., Olivier, A. & Amblard, J. MHD-control on limiting Faradaic currents. *Energy Convers. Manag.* **43,** 365–371 (2002).
2. Legeai, S., Chatelut, M., Vittori, O., Chopart, J.-P. & Aaboubi, O. Magnetic field influence on mass transport phenomena. *Electrochim. Acta* **50,** 51–57 (2004).
3. Lee, J., Ragsdale, S. R., Gao, X. & White, H. S. Magnetic field control of the potential distribution and current at microdisk electrodes. *J. Electroanal. Chem.* **422,** 169–177 (1997).
4. Bund, A., Koehler, S., Kuehnlein, H. H. & Plieth, W. Magnetic field effects in electrochemical reactions. *Electrochim. Acta* **49,** 147–152 (2003).
5. Olivier, A., Chopart, J., Amblard, J., Merienne, E. & Aaboubi, O. Direct & indirect electrokinetic effect inducing a forced convection . Ekhd & mhd transfer functions. *ACH - Model. Chem.* **137,** 213–224 (2000).
6. Devos, O. *et al.* Is There a Magnetic Field Effect on Electrochemical Kinetics? *J. Phys. Chem. A* 1544–1548 (2000).
7. Rhen, F. M. F., Fernandez, D., Hinds, G. & Coey, J. M. D. Influence of a Magnetic Field on the Electrochemical Rest Potential. *J. Electrochem. Soc.* **153,** J1 (2006).
8. Chiba, A., Ogawa, T. & Yamashita, T. Magnetic field effects on the electrodeposition of copper from copper sulphate in sulphuric acid. *Surf. Coatings Technol.* **34,** 455–462 (1988).
9. Sagawa, M. Effect of a Local Magnetic Field on the Dissolution of Copper and Iron in Nitric Acid Solution. *Trans. Japan Inst. Met.* **23,** 38–40 (1982).
10. Sueptitz, R., Tschulik, K., Uhlemann, M., Schultz, L. & Gebert, A. Magnetic field effects on the active dissolution of iron. *Electrochim. Acta* **56,** 5866–5871 (2011).
11. Ragsdale, S. R., Lee, J., Gao, X. & White, H. S. Magnetic Field Effects in Electrochemistry. Voltammetric Reduction of Acetophenone at Microdisk Electrodes. *J. Phys. Chem.* **100,** 5913–5922 (1996).
12. Ragsdale, S. R., Grant, K. M. & White, H. S. Electrochemically Generated Magnetic Forces. Enhanced Transport of a Paramagnetic Redox Species in Large, Nonuniform Magnetic Fields. *J. Am. Chem. Soc.* **120,** 13461–13468 (1998).
13. Fahidy, T. Z. Hydrodynamic models in magnetorelectrolysis. *Electrochim. Acta* **18,** 607–614 (1973).
14. Tacken, R. . & Janssen, L. J. . Applications of magnetoelectrolysis. *J. Appl. Electrochem.* **25,** 1–5 (1995).
15. Krogstad, H. N. & Johnsen, R. Galvanic Corrosion of Nickel Aluminium Bronze Exposed to Seawater in a Magnetic Field. in *CORROSION 2016 Paper No. 7451* (2016).
16. Krogstad, H. N. & Johnsen, R. Corrosion properties of nickel-aluminium bronze in natural seawater - Effect of galvanic coupling to UNS S31603. *Corros. Sci.* **121,** 43–56 (2017).
17. Faraday, M. *Diary Vol. IV*. (Bell & Sons, 1933).
18. Aogaki, R., Fueki, K. & Mukaibo, T. Application of magnetohydrodynamic effect to the analysis of electrochemical reactions-2. Diffusion process in MHD forced flow of electrolyte solutions. *Denki Kagaku* **9,** 509–514 (1975).
19. Aaboubi, O. *et al.* Magnetic Field Effects on Mass Transport. *J. Electrochem. Soc.* **137,** 1796 (1990).
20. Chopart, J. P., Douglade, J., Fricoteaux, P. & Olivier, A. Electrodeposition and Electrodissolution of Copper with a Magnetif Field: Dynamic and Stationary Investigations. *Electrochim. Acta* **36,** 459–463 (1991).
21. Lee, J., Gao, X., Hardy, L. & White, H. S. Influence of magnetic fields on the voltammetric response of microelectrodes in highly concentrated organic redox solutions. *J. electrochmical Soc.* **142,** (1995).
22. Ragsdale, S. R., Lee, J. & White, H. S. Analysis of the magnetic force generated at a hemispherical microelectrode. *Anal. Chem.* **69,** 2070–6 (1997).
23. Brien, R. N. O. & Santhaman, K. S. V. Magnetic field assisted convection in an electrolyte of nonuniform magnetic susceptibility. *J. Appl. Electrochem.* **27,** 573–578 (1997).
24. Leventis, N., Chen, M., Gao, X., Canalas, M. & Zhang, P. Electrochemistry with Stationary Disk and Ring–Disk Millielectrodes in Magnetic Fields. *J. Phys. Chem. B* **102,** 3512–3522 (1998).
25. Monzon, L. M. A. & Coey, J. M. D. Magnetic fields in electrochemistry: The Lorentz force. A mini-review. *Electrochem. commun.* **42,** 38–41 (2014).
26. Mohanta, S. & Fahidy, T. Z. The Effect of a Uniform Magnetic Field on Mass Transfer in Electrolysis. *Can. J. Chem. Eng.* **50,** 248–253 (1972).
27. Grant, K. M., Hemmert, J. W. & White, H. S. Magnetic focusing of redox molecules at ferromagnetic microelectrodes. *Electrochem. commun.* **1,** 319–323 (1999).
28. Monzon, L. M. A. & Coey, J. M. D. Magnetic fields in electrochemistry: The Kelvin force. A mini-review. *Electrochem. commun.* **42,** 42–45 (2014).
29. Fricoteaux, P. Study of the Exchange Current at the Cu2+/Cu

Interface by Radiotracer: Magnetic Field Effect. *J. Electrochem. Soc.* **139,** 1096 (1992).

30. Hinds, G. Magnetic field effect of electrodeposition and electrodissolution of copper. (University of Dublin, 2000).

31. Kelly, E. J. Magnetic Field Effects on Electrochemical Reactions Occurring at Metal/Flowing-Electrolyte Interfaces. *J. Electrochem. Soc.* **124,** 987 (1977).

32. Iwakura, C., Kitayama, M., Edamoto, T. & Tamura, H. The fundamental studies on the development of a new electrolysis method: magnetoelectrolysis. *Electrochim. Acta* **30,** 747–752 (1985).

33. Grant, K. M., Hemmert, J. W. & White, H. S. Magnetic focusing of redox molecules at ferromagnetic microelectrodes. *Electrochem. commun.* **1,** 319–323 (1999).

34. Dass, A., Counsil, J. a, Gao, X. & Leventis, N. Magnetic field effects on the open circuit potential of ferromagnetic electrodes in corroding solutions. *J. Phys. Chem. B* **109,** 11065–73 (2005).

35. Dunne, P. & Coey, J. M. D. Patterning metallic electrodeposits with magnet arrays. *Phys. Rev. B - Condens. Matter Mater. Phys.* **85,** 1–21 (2012).

36. Hinds, G., Coey, J. M. D. & Lyons, M. E. G. Influence of magnetic forces on electrochemical mass transport. *Electrochem. commun.* **3,** 215–218 (2001).

37. Waskaas, M. & Kharkats, Y. I. Effect of magnetic fields on convection in solutions containing paramagnetic ions. **502,** 51–57 (2001).

38. Coey, J. M. D., Rhen, F. M. F., Dunne, P. & McMurry, S. The magnetic concentration gradient force-Is it real? *J. Solid State Electrochem.* **11,** 711–717 (2007).

39. Meigh, H. *Cast and Wrought Aluminium Bronzes*. (2000).

40. Danan, H., Herr, A. & Meyer, J. P. New Determinations of the Saturation Magnetization of Nickel and Iron. *J. Appl. Phys.* **39,** 669–670 (1968).

41. Hasan, F., Lorimer, G., Ridley, N. & Jahanafrooz, A. The morphology, crystallography, and chemistry of as-cast nickel-aluminium bronze. *Metall. Mater. Trans. A* **13,** 1337–1345 (1982).

42. Culpan, E. A. & Rose, R. Corrosion Behaviour of Cast Nickel Aluminum Bronze in Sea Water. *Br. Corros. J.* 160–166 (1979).

43. Wharton, J. A. *et al.* The corrosion of nickel-aluminium bronze in seawater. *Corros. Sci.* **47,** 3336–3367 (2005).

44. Wharton, J. A. & Stokes, K. R. The influence of nickel–aluminium bronze microstructure and crevice solution on the initiation of crevice corrosion. *Electrochim. Acta* **53,** 2463–2473 (2008).

45. Al-Hashem, A., Caceres, P. G., Riad, W. T. & Shalaby, H. M. Cavitation Corrosion Behavior of Cast Nickel-Aluminum Bronze in Seawater. *CORROSION* **51,** 331–342 (1995).

46. Neodo, S., Carugo, D., Wharton, J. A. & Stokes, K. R. Electrochemical behaviour of nickel–aluminium bronze in chloride media: Influence of pH and benzotriazole. *J. Electroanal. Chem.* **695,** 38–46 (2013).

47. Kear, G., Barker, B. D. & Walsh, F. C. Electrochemical corrosion of unalloyed copper in chloride media-a critical review. *Corros. Sci.* **46,** 109–135 (2004).

48. Crousier, J., Pardessus, L. & Crousier, J. P. Voltammetry study of copper in chloride solution. *Electrochim. Acta* **33,** 1039–1042 (1988).

49. Yuan, B., Wang, C., Li, L. & Chen, S. Investigation of the effects of the magnetic field on the anodic dissolution of copper in NaCl solutions with holography. *Corros. Sci.* **58,** 69–78 (2012).

50. Faita, G., Fiori, G. & Salvadore, D. Copper behaviour in acid and alkaline brines-I kinetics of anodic dissolution in 0.5M NaCl and free-corrosion rates in the presence of oxygen. *Corros. Sci.* **15,** 383–392 (1975).

51. Al-Abdallah, M. M., Maayta, a. K., Al-Qudah, M. a. & Al-Rawashdeh, N. a. F. Corrosion Behavior of Copper in Chloride Media. *Open Corros. J.* **2,** 71–76 (2009).

52. Schüssler, A. & Exner, H. E. The Corrosion of Nickel-Aluminium Bronze in Seawater-I. Protective Layer Formation and the Passivation Mechanism. *Corros. Sci.* **34,** 1793–1802 (1993).

53. Pletcher, D., Graff, R., Peat, R., Peter, L. M. & Robinson, J. in *Instrumental Methods in Electrochemistry* 113–148 (2010). doi:10.1533/9781782420545.113

54. Kear, G., Barker, B. D., Stokes, K. & Walsh, F. C. Flow influenced electrochemical corrosion of nickel aluminium bronze - Part II. Anodic polarisation and derivation of the mixed potential. *J. Appl. Electrochem.* **34,** 1235–1240 (2004).

55. Kear, G., Barker, B. D., Stokes, K. & Walsh, F. C. Flow influenced electrochemical corrosion of nickel aluminium bronze - Part I. Cathodic polarisation. *J. Appl. Electrochem.* **34,** 1235–1240 (2004).